State Estimation for Cardiac Action Potential Dynamics: A Comparison of Kalman Filter Designs

Laura M Muñoz, Christopher B Beam

School of Mathematical Sciences, Rochester Institute of Technology, Rochester, NY, USA

Abstract

Various technologies, such as electrocardiography, optical mapping, and patch clamping, have been developed to monitor cardiac electrophysiological behavior in live tissue. One limitation is that none of the available measurement methods is capable of monitoring simultaneously all quantities, such as intracellular ionic concentrations and ion-channel gating states, that may be important contributors to arrhythmia formation. Data assimilation strategies such as Kalman filtering can be used to fill in missing measurements, but to our knowledge, there have been few comparisons of different state estimation algorithms applied to the same cardiac action potential model.

To help develop a framework for comparing performances of estimators, we applied two estimation algorithms, an unscented Kalman filter (UKF) and a gain-scheduled Kalman filter (GSKF), to a two-variable Karma model of a cardiac cell. We generated simulated data from the model and compared the abilities of the algorithms to infer the slow variable of the model from measurements of the fast variable and vice versa. The UKF performed well when the process noise variance was low relative to measurement noise, while the opposite was often true for the GSKF, and estimation errors tended to be smaller when the fast variable was chosen as the measurement.

1. Introduction

Data assimilation methods, including state estimation algorithms based on the Kalman filter (KF) [1], can be used to reconstruct quantities that are difficult or impossible to measure directly. These algorithms combine models with data, typically by using available measurements to correct predictions obtained from a dynamical model of the system of interest. KF-based estimators have been applied to body-level cardiac measurements such as electrocardiographic data [2, 3]. Some studies have applied state estimators or related algorithms called observers to tissue or cell-level models (see [4–6] for examples). Typically, these studies have focused on one type of estimation algorithm, and to our knowledge there have been few comparisons of different estimation algorithms on the same cardiac action potential (AP) model, though such comparisons have been made for other types of models [7]. Hence, we decided to compare the abilities of two data assimilation algorithms, an unscented Kalman filter (UKF) [8] and a gain-scheduled Kalman filter (GSKF) design on the Karma two-variable model of a cardiac cell [9, 10]. We selected a nonlinear estimator, the UKF, since the UKF and its extensions have been applied successfully to models of neurons [7] and cardiac tissue [5]. The GSKF design, which in this instance relies on feedback gains updated at regular intervals within each period, was of interest because of its simplicity, along with the observation that certain linear feedback methods have shown promise in related studies on alternans suppression [11]. The Karma model was chosen as a starting point for filter designs and comparisons due to its low dimensionality and ability to represent physiological phenomena of interest, such as alternans. We used both filters to estimate the slow variable of the Karma model from noise-corrupted simulated measurements of the fast variable, then estimated the fast variable from the slow variable, and examined the impact of different noise ratios and periods on filter performance.

2. Methods

The two-variable Karma model [9, 10] of a single cell may be written as $\dot{X} = f(X,t)$, where the system state vector is defined as $X = [V\ w]^T$, $V(t)$ is the membrane potential (in mV) at time t, $w(t)$ is the refractory variable (dimensionless). The equations are

$$\dot{V} = \frac{1}{\tau_V} f_1(V,w) - I_{stim}/C_m, \quad \dot{w} = \frac{1}{\tau_w} f_2(V,w), \quad (1)$$

where the stimulus current $I_{stim}(t)$ is a rectangular pulse with period T, amplitude -32 μA cm^{-2}, and duration 2.5 ms. f_1 and f_2 are defined as

$$f_1(V,w) = -V - V_b + (\nu - w^M)\left(\sum\nolimits_{\iota=0}^{3} c_\iota V^\iota\right),$$

$$f_2(V,w) = \frac{1}{2b}(1 + \tanh(V - V_w)) - w,$$

 ISSN: 2325-887X DOI: 10.22489/CinC.2020.465

where a Heaviside function in the original model was replaced with a hyperbolic tangent to aid in computing Jacobians, $M = 10$, $b = 0.7059$, and other parameter values (C_m, τ_w, V_b, ν, c_t, V_w) were adapted from [12]. The model exhibits steep depolarization, which is reflective of Purkinje fiber AP behavior but presents challenges for linearization. Here, τ_V was set to 20 ms (default is 5 ms) to yield more gradual transitions.

The model was forward-Euler integrated with time step $dt = 0.01$ ms from initial condition X_0. The resulting model-generated state $X(t)$ was considered to be the "true" system state. The simulated measurement was $Y = CX + r$, where $r(t)$ was zero-mean normally-distributed noise with variance R, produced with the `randn` function in Matlab at each dt interval throughout the simulation. Estimating w based on measurements of V (indicated by $C = [1\ 0]$) was of greater interest than estimating V from measurements of w, since V is often accessible in a lab setting, whereas w indicates the refractory state of the cell rather than directly representing a measurable quantity. However, $C = [0\ 1]$ was also examined.

The 2×2 process noise covariance matrix Q was used as a design parameter for both filters; large Q indicates high uncertainty in the model's predictions, whereas small Q indicates low uncertainty. Typically, Q would represent the covariance of a zero-mean normally-distributed process noise signal $q(t)$ that is injected into the model, for example, by adding it to the right side of the forward-Euler discretized version of Eq. (1). However, the Karma model was found to be sensitive (X sometimes grows without bound) to sufficiently large process noise injections, hence $q(t)$ was not included in the dynamical equations, yet Q was retained as a design parameter.

Gain scheduling typically refers to a class of feedback design methods where a limited number of feedback gains are computed for selected points within the state space, and the feedback term switches among these gains according to specified transition rules. Here, gains were calculated for a number, K, of points along a reference trajectory, $X_r(t)$, which was produced by integrating Eq. (1) from an initial guess $X_{r,0} = [-84.55\ 0.7064]^T$, chosen near a period-1 trajectory of the model for $T = 300$ ms. The true initial state was chosen as a randomly perturbed version of the initial guess via $X_0 = X_{r,0} + p$, where p is a normally-distributed 2×1 random vector with zero mean and covariance P, which was set to a diagonal matrix with default diagonal entries of 20 and 0.2.

To set up the GSKF for a simulation spanning N periods ($j = 0, 1, ..., N-1$), each period was divided into K uniformly-spaced subdivisions of duration ΔT indexed by $k = 0, 1, ..., K-1$. In general, $\Delta T > dt$. Starting at $j = 1$, the GSKF calculates state estimates according to $\hat{X}_m = X_{r,m} + \hat{x}_m$, where $m = (j-1)K + k$ and the deviational state estimate $\hat{x}$ is computed with:

$$\hat{x}_{m+K} = A_k \hat{x}_m + L_k \epsilon_m \tag{2}$$

The residual is $\epsilon_m = Y_m - C\hat{X}_m$. This particular GSKF is a collection of linear-time-invariant filters, each of which is a period-1 estimator based on the standard Kalman filter; the filters are just initiated at different times along an AP profile. Initial conditions were $\hat{x}_m = 0$ for $m = 0, 1, ..., K-1$. A_k is the state transition matrix from one period to the next, initiated at the k-th subdivision. To compute A_k, we evaluated the Jacobian of Eq. (1) along X_r for the first period in the simulation, where Jacobians over time scale dt were computed explicitly by differentiating the forward-Euler discretized version of Eq. (1) with respect to its state variables. A_k was then the product of dt-scale Jacobians covering the first period. Gains L_k were obtained based on A_k, C, Q, and R using the `kalman` function in Matlab. A_k and L_k repeat periodically, whereas state estimates and residuals were updated throughout the simulation. In cases where V was the measurement, rapid changes in gain sometimes destabilized the GSKF, hence a gain hold was imposed where $L_{k,i}$, the i-th component of L_k, was maintained at its most recent value in cases where $|L_{k+1,i} - L_{k,i}| > \gamma_i$, where $\gamma_1 = 0.2$ and $\gamma_2 = 1$, and $i \in \{1, 2\}$ is the state variable index.

The UKF computes state estimates and covariances by direct application of model equations to a collection of specially-chosen points in the state space called sigma points. We used Matlab's `unscentedKalmanFilter` function, with default settings, to implement the UKF based on C, Q, R and the forward-Euler version of Eq. (1). The initial guess for the UKF was $X_{r,0}$. The UKF produced state estimates $\hat{X}$ at every Euler time step.

Mean absolute relative estimation errors were computed as follows for each state variable:

$$E_{filt,i} = \frac{1}{M_E} \sum\nolimits_{m=m_{ini}}^{m_{fin}} |(X_{i,m} - \hat{X}_{i,m})/X_{i,m}|$$

where $filt$ refers to either the GSKF or the UKF, and errors were evaluated over $m \in \{m_{ini} \ldots m_{fin}\}$, where the initial and final indices were chosen to cover the last four cycles for a total of M_E subdivisions.

3. Results and Discussion

The estimators were tested at $T = 300$ and 500 ms for two noise ratios, $||Q||/R = 10^6$ and 10^{-6}. Q was chosen as a diagonal matrix with diagonal entries Q_1 and Q_2. When V was the measured variable, the high $||Q||/R$ case corresponded to $Q_1 = 50$, $Q_2 = 0.5$, $R = 5 \times 10^{-5}$, and for the low $||Q||/R$ case, $Q_1 = 5 \times 10^{-6}$, $Q_2 = 5 \times 10^{-8}$, $R = 5$. When w was the measured variable, all the Q_i and R values listed previously were divided by 2000, which

preserved $||Q||/R$ ratios but yielded measurement noise that was more proportionate to w. Each estimator was run for $N = 10$ periods, where the GSKF used $K = 10$ subdivisions per period. For $T = 300$ ms, X_r is close to period-1 while X exhibits transient alternans, but at $T = 500$ ms, both trajectories settle quickly into a period-1 rhythm.

State estimates are shown for $T = 300$ ms for the two $||Q||/R$ cases, where w was estimated from V in Figures 1 and 2 and for V estimated from w in Figures 3 and 4. Estimation errors for the two measurement scenarios are summarized in Tables 1 and 2. UKF results were not available (labeled N/A in Table 2) for the high $||Q||/R$ cases where w was measured due to a sigma-point calculation failure of the algorithm. The figures and tables show that the UKF estimated the unmeasured state accurately when $||Q||/R$ was low. This is consistent with both true and measured trajectories being generated from the same model, but if V data from a real cell had been used instead, for certain measurement devices such as microelectrodes, we would expect the opposite scenario (high $||Q||/R$) to be more realistic since the data would likely be more reliable than the model. For $T = 300$ ms, the GSKF estimates were more accurate for high $||Q||/R$ (stronger feedback) compared with low $||Q||/R$ for either measurement type, but there was no benefit to stronger feedback at $T = 500$ ms.

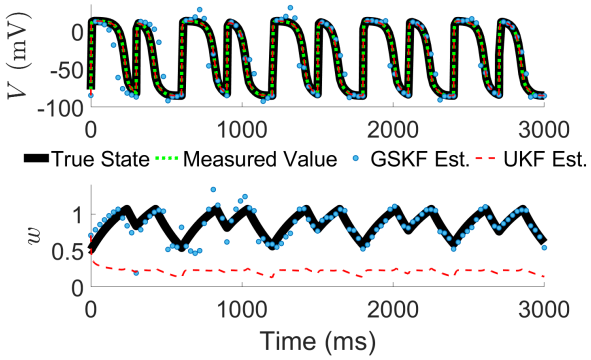

Figure 1. Estimates of state variables from the GSKF and UKF, along with true state variables and measured V, for $T = 300$ ms, for high $||Q||/R$.

Table 1. Mean absolute relative estimation errors for w based on measurements of V.

T (ms)	$\|\|Q\|\|/R$	$E_{GSKF,w}$	$E_{UKF,w}$
500	high	0.0004	0.7414
500	low	0.0004	0.0031
300	high	0.0512	0.7532
300	low	0.1079	0.0028

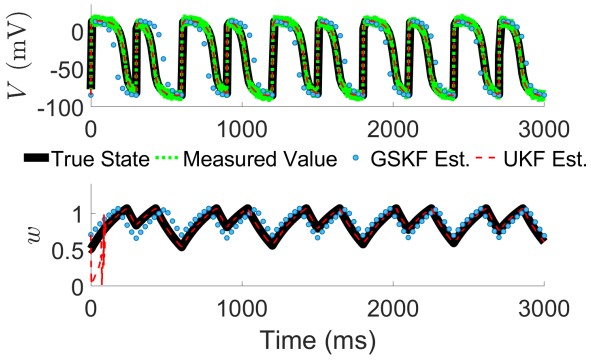

Figure 2. Estimates of state variables from the GSKF and UKF, along with true state variables and measured V, for $T = 300$ ms, for low $||Q||/R$.

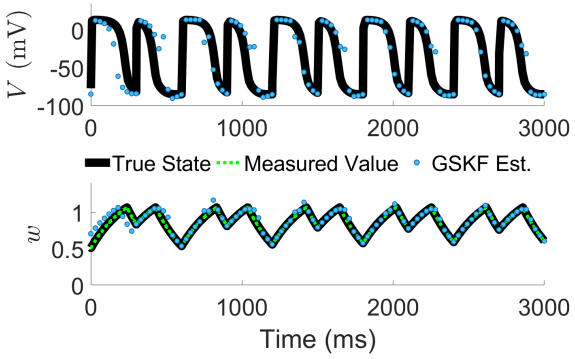

Figure 3. Estimates of state variables from the GSKF, along with true state variables and measured w, for $T = 300$ ms, for high $||Q||/R$.

The tables show that relative errors were typically larger when V was estimated from w rather than the reverse. This appears to be consistent with our earlier result [13], which indicated that measuring V yielded stronger observability than measuring w in the Karma model (in other words, it was determined that reconstructing w from V would be easier than reconstructing V from w).

A number of limitations apply to the work. Extreme noise ratio settings were chosen to highlight differences. Testing scenarios with a two-variable model was intended as a starting point for extensions to higher-dimensional systems that represent at least several distinct measurable quantities, such as models that represent membrane potential at multiple locations within a spatially distributed system and/or ionic concentrations in addition to membrane potential. The GSKF is expected to perform more reliably when K is sufficiently small, whereas the UKF can update estimates more frequently. The GSKF requires a reference trajectory and presumably will yield better performance when X_r is initiated near a point along a period-

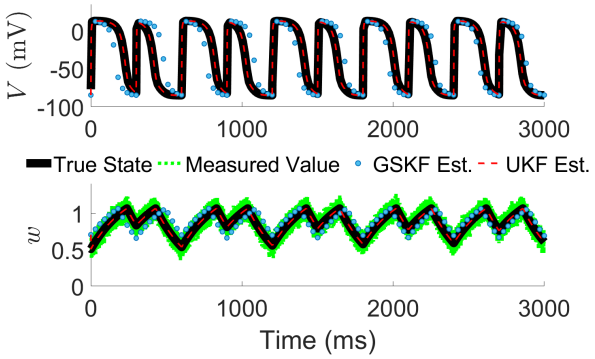

Figure 4. Estimates of state variables from the GSKF and UKF, along with true state variables and measured w, for $T = 300$ ms, for low $||Q||/R$.

Table 2. Mean absolute relative estimation errors for V based on measurements of w.

T (ms)	$\|\|Q\|\|/R$	$E_{GSKF,V}$	$E_{UKF,V}$
500	high	0.0017	N/A
500	low	0.0015	0.0011
300	high	0.3314	N/A
300	low	0.8213	0.0031

1 trajectory for the given T, since steady-state methods were used to compute the L_k gains. Many other gain-scheduling methods and filter designs besides the ones shown here could have been considered. The GSKF, which in its present form is not expected to work well for complex trajectories involving large deviations between X and X_r, is not being offered as an advancement over the UKF, but rather as a basis for comparison (benchmark) that we expect to be compatible with certain systems design and analysis tools, such as linear observability analysis, which could aid in understanding of conditions that yield better filter performance.

4. Conclusions

An unscented KF and a gain-scheduled KF were tested on a two-variable nonlinear model of a cardiac cell under different period, noise ratio, and measurement conditions. The UKF tended to produce more accurate estimates when process noise was low compared to measurement noise, whereas the GSKF was more accurate for higher process noise for the shorter of the two periods examined. In most cases, estimating w from measurements of V yielded lower estimation errors than estimating V from measurements of w, for either filter.

References

[1] Kalman R. A new approach to linear filtering and prediction problems. Transactions of the ASME Journal of Basic Engineering 1960;82(1):35–45.

[2] Szilagyi L. Application of the Kalman filter in cardiac arrhythmia detection. In Proceedings of the 20th Annual International Conference of the IEEE Engineering in Medicine and Biology Society. Vol. 20 Biomedical Engineering Towards the Year 2000 and Beyond (Cat. No.98CH36286). Hong Kong, China: IEEE, 1998; 98–100.

[3] Wang L. Computational reduction for noninvasive transmural electrophysiological imaging. Computers in Biology and Medicine March 2013;43(3):184–199. ISSN 00104825.

[4] Dubljevic S, Lin SF, Christofides PD. Studies of feedback control of cardiac alternans. Comp Chem Eng 2008; 32:2086–2098.

[5] LaVigne NS, Holt N, Hoffman MJ, Cherry EM. Effects of model error on cardiac electrical wave state reconstruction using data assimilation. Chaos An Interdisciplinary Journal of Nonlinear Science September 2017;27(9):093911. ISSN 1054-1500, 1089-7682.

[6] Guzman A, Vogt R, Charron C, Pusarla K, Muñoz L. Observability analysis and state observer design for a cardiac ionic cell model. Computers in Biology and Medicine July 2020;103910. ISSN 00104825.

[7] Voss HU, Timmer J, Kurths J. Nonlinear dynamical system identification from uncertain and indirect measurements. International Journal of Bifurcation and Chaos June 2004; 14(06):1905–1933. ISSN 0218-1274, 1793-6551.

[8] Julier SJ, Uhlmann JK. New extension of the Kalman filter to nonlinear systems. In SPIE 3068, Signal Processing, Sensor Fusion, and Target Recognition VI. 1997; 182–193.

[9] Karma A. Spiral breakup in model equations of action potential propagation in cardiac tissue. Physical Review Letters August 1993;71(7):1103–1106. ISSN 0031-9007.

[10] Karma A. Electrical alternans and spiral wave breakup in cardiac tissue. Chaos 1994;4(3):461–479.

[11] Garzón A, Grigoriev RO, Fenton FH. Continuous-time control of alternans in long Purkinje fibers. Chaos An Interdisciplinary Journal of Nonlinear Science September 2014; 24(3):033124. ISSN 1054-1500, 1089-7682.

[12] Rappel WJ, Fenton F, Karma A. Spatiotemporal control of wave instabilities in cardiac tissue. Physical Review Letters July 1999;83(2):456–459. ISSN 0031-9007, 1079-7114.

[13] Muñoz LM, Otani NF. Enhanced computer modeling of cardiac action potential dynamics using experimental data-based feedback. In Computing in Cardiology, volume 37. 2010; 837–840.

Address for correspondence:

Laura Muñoz
Rochester Institute of Technology
85 Lomb Memorial Drive
Rochester, NY, USA, 14623
laura.m.munoz@gmail.com